Available online at www.sciencedirect.com
ScienceDirect
Journal of Magnetic Resonance 187 (2007) 57–65
JMR Journal of Magnetic Resonance
www.elsevier.com/locate/jmr

Transverse oriented electric field re-entrant resonator (TERR) with automatic tuning and coupling control for EPR spectroscopy and imaging of the beating heart

Guanglong He *, Cristian Dumitrescu, Sergey Petryakov, Yuanmu Deng, Eric Kesselring, Jay L. Zweier *

The Center for Biomedical EPR Spectroscopy and Imaging, Davis Heart and Lung Research Institute, and Division of Cardiology, Department of Internal Medicine, The Ohio State University College of Medicine, Columbus, OH 43210, USA

Received 14 November 2006; revised 15 March 2007
Available online 12 April 2007

Abstract

Sample motion, particularly that of a beating heart, induces baseline noise and spectral distortion on an EPR spectrum. In order to quench motional noise and restore the EPR signal amplitude and line-width, an L-band transverse oriented electric field re-entrant resonator (TERR) was designed and constructed with provisions for automatic tuning control (ATC) and automatic coupling control (ACC) suited for studies of isolated beating rat hearts. Two sets of electronic circuits providing DC biased voltage to two varactor diodes were implemented to electronically adjust coupling and tuning. The resonator has a rectangular cross-sectional sample arm of 25 mm diameter with a Q value of 1100 without sample. Once inserted with lossy aqueous samples of 0.45% NaCl, Q value drops to 400 with a volume of 0.5 ml and 150 with 5 ml. The ATC/ACC functions were tested with a moving phantom and isolated beating rat hearts with the improvement of signal to noise ratio (S/N, peak amplitude of signal over peak amplitude of baseline noise) of 6.7-, and 4 to 6-fold, respectively. With these improvements, EPR imaging could be performed on an isolated beating rat heart. Thus, this TERR resonator with ATC/ACC enables application of EPR spectroscopy and imaging for the measurement and imaging of radical metabolism, redox state, and oxygenation in the isolated beating rat heart.

Keywords: EPR spectroscopy and imaging; Microwave resonator; Noise reduction; ATC/ACC; Isolated heart; Nitroxyl radical

1. Introduction

EPR spectroscopy (EPR) and imaging (EPRI) has been applied to measure the generation and distribution of free radicals in biological systems [1–12]. Among various applications, it has been particularly challenging to measure and image free radicals in the beating heart due to its lossiness and motion [13–15]. With lumped circuit resonator designs, *in vivo* and *ex vivo* EPR/EPRI was made possible at low frequency from S-band down to 250 MHz on lossy biological samples as well as on moving objects with feedback control circuits for AFC/ATC [16–25]. Similar resonator designs have also been applied to the field of nuclear magnetic resonance imaging [26–28]. However, cardiac and respiratory motion induces baseline instability and line-width distortion that limit the sensitivity, spectral accuracy, and imaging resolution that can be obtained. Since the conventional automatic frequency control (AFC) technique tracks and locks the frequency of the oscillator to the frequency of the resonator, when the resonator is inserted with a moving sample, the frequency and impedance of the resonator changes accordingly and thereby induces motional noise. This motion-induced noise often limits

* Corresponding authors. Address: 473 W. 12th Avenue, Columbus, OH 43210-1252, USA. Fax: +1 614298454.
E-mail addresses: Guanglong.He@osumc.edu (G. He), Jay.Zweier@osumc.edu (J.L. Zweier).

1090-7807/$ - see front matter © 2007 Elsevier Inc. All rights reserved.
doi:10.1016/j.jmr.2007.03.020

the detection and assessment of the signal intensity and the line-width of an EPR spectrum or image projection due to reduction in S/N and distorted line shape. The resultant EPR spectra or image projections are superimposed with the noise derived from the change of tuning and coupling of the resonator. Therefore, it is extremely important to develop techniques to suppress motional noise.

In order to quench motional noise for CW EPR, it is necessary to develop electronic tuning and coupling mechanisms to track and adjust the frequency of the resonator to the frequency of the oscillator, and also provide impedance transformation between the resonator and transmission line to fix the detector bias in the microwave bridge. Varactor diodes are commonly used components with a relatively fast time response to adjust the capacitance of the tuning and coupling mechanisms. When biased with a DC correction voltage signal from the ATC/ACC circuits, they enable locking the resonator frequency and impedance to that of the microwave bridge [22]. In addition, feedback electronic circuits have to be implemented to track and correct the tuning and coupling shifts of the resonator.

In order to accommodate different biological samples, different resonator designs have to be used to maximize the coupling capacity, filling factor, and the S/N. To perform EPR/EPRI on an isolated beating rat heart, special design and construction of the resonator is required to work at a frequency as high as possible with an appropriate dimension to accommodate the rat heart which then will give an optimized filling factor for maximizing the EPR signal intensity. It was observed that a frequency range of L-band (1–2 GHz) provided good sensitivity and adequate microwave penetration for EPR/EPRI of the beating rat heart [29–31].

It was previously reported that at low frequencies from 250 MHz to L-band, resonator designs with ATC/ACC techniques can quench motional noise from different biological samples [20,22,32]. We have previously reported that the TERR design can provide a tunable high Q structure well suited for *in vivo* EPR spectroscopy. It can also allow the incorporation of ATC and ACC provisions. Earlier TERR designs were developed at frequencies below 750 MHz for *in vivo* whole body mouse applications [22]. However, adapting the ATC/ACC technique from a lower frequency of 750 MHz to a higher frequency L-band resonator design is not a trivial process. It involves applying the similar technique to a smaller resonator with higher sensitivity. Generally, the higher the frequency of the resonator and the smaller its size, the more sensitive it is to motion-induced noise. A resonator with higher sensitivity at higher frequency will also pick up more motional noise which imposes a greater challenge for techniques aiming at quenching this noise. Therefore, adapting the ATC/ACC provisions and TERR design for L-band applications is an important step and much needed development for *in vivo* and *ex vivo* EPR imaging applications. There have been no prior reports on the design of volume resonators suitable for EPR imaging at L-band with provisions for ATC/ACC. Thus, prior measurements of moving biological samples such as the heart have been greatly limited by motion-induced noise. The development of a TERR resonator with ATC/ACC provisions at L-band provides a solution to this problem and can enable high sensitivity EPR spectroscopy and imaging needed to measure and image free radicals in the isolated beating rat heart.

In the current paper, we describe a TERR resonator design at L-band with ATC/ACC provisions suited to perform EPR/EPRI on an isolated beating heart. The resonator has a homogeneous distribution of B_1 field over a cylindrical volume of 20 mm in length and 20 mm in diameter, which is required for imaging a rat heart. With the ATC/ACC provisions, the EPR S/N was improved 6.7 times on a moving phantom and over 4 times on an isolated beating rat heart. Thus, this TERR resonator design with ATC/ACC provisions, enables improved EPR spectroscopy and imaging measurements of free radicals in the isolated beating rat heart.

2. Resonator design

2.1. Tuning and coupling mechanism

Previously, we have reported the design and construction of a TERR resonator at 750 MHz to perform EPR/EPRI measurements on whole body small animals [22]. A similar strategy was used in the current design of the L-band TERR resonator with copper-clad epoxy-glass laminate material (copper-clad G-10/FR4 Garolite, McMaster-CARR) as the building blocks for the resonator walls. The copper-clad building blocks were silver-plated to improve the conductivity and therefore the Q value of the resonator. The resonator was a rectangular box and the dimensions and specifications are shown in Fig. 1A and Table 1. A central stationary copper plate plated with silver was attached to one side of the resonator to serve as the stationary capacitive tuning and coupling plates. At the end of the central conductor of the transmission line, a small silver-plated copper disc serving as the coupling plate was attached and was pivoted by a micro positioner to couple the resonator to a desired sample volume (Fig. 1B). A silver-plated copper strip attached to the opposite wall serves as the tuning plate and is pressed with a quartz rod pivoted by another positioner to change the relative position of the tuning plate with respect to the central stationary plate to tune the resonator to the microwave oscillator. The frequency of the resonator was centered at 1.2 GHz and the mechanical tuning range was 100 MHz (1.2 GHz $\pm$ 50 MHz) with a Q value of 1100 without sample. Fig. 1 shows the photograph of the L-band TERR resonator with a pair of modulation coils mounted on the outside walls. Brass tubes were attached to the ends of the sample holder as shields to prevent microwave leakage. The figure also shows the two positioning mechanisms to control the tuning and coupling of the resonator.

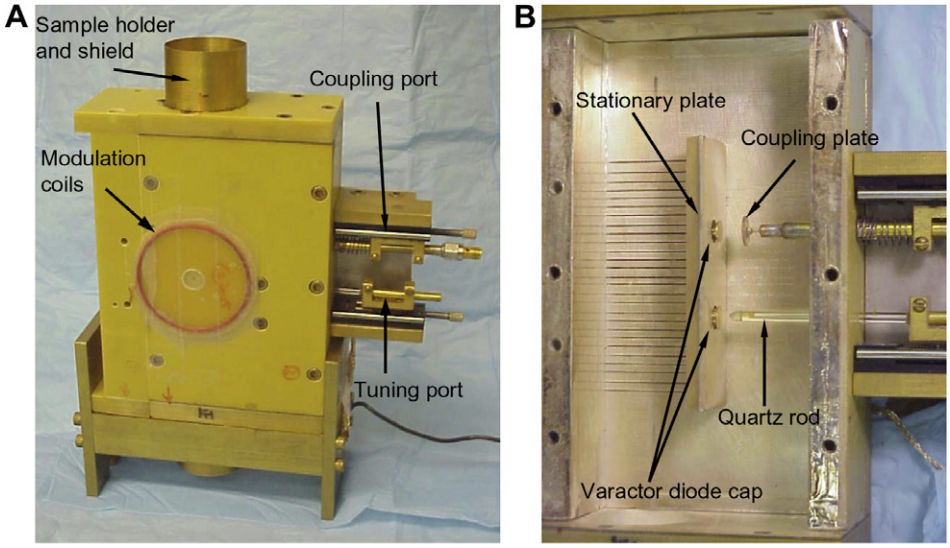

Fig. 1. Photograph showing the external and internal structure of the L-band TERR resonator. (A) The arrows indicate the exterior modulation coils, sample holders, tuning and coupling ports. (B) The interior structure of the TERR is shown after opening with removal of the wall containing the movable capacitive tuning plate. The arrows indicate stationary plate, coupling plate, (tuning) quartz rod, and varactor diode cap. The movable capacitive tuning plate is not seen as it is attached to the removed wall. In the closed resonator this plate from the opposite wall abuts on the tuning quartz rod.

Table 1
Specifications of the L-band TERR resonator

Parameter	Value
Overall dimensions outside (mm)	$85 \times 154 \times 49$
Dimensions inside (mm)	$65 \times 134 \times 29$
Sample arm opening (mm)	25
Center frequency (MHz)	1200
Center frequency (calculated) (MHz)	1250
Center frequency setting range (MHz)	1000–1500
Center frequency tuning range (MHz)	± 50
Q value before insertion of varactor diodes	2400
Q value without sample	1100
Q value with 0.5 ml 0.45% PBS	400
Maximum aqueous volume coupling capacity (ml)	10

2.2. Placement of the varactor diodes

Two wells of 5 mm diameter were machined in the central stationary plate underneath the coupling and tuning plates, respectively. Two varactor diodes (high Q hyperabrupt tuning varactor, MA4ST553-31, M/A-COM Inc.) were attached to the bottom of the wells with silver conductive glue [22]. They were each capped with a small metal disc to form another capacitor with the tuning and coupling plates to couple the microwave energy to the varactor diodes (shown in Fig. 1B). Upon insertion of the varactor diodes, the Q value dropped from 2400 to 1100 due to the relatively lower Q value of the varactor diodes (500 at -4 V bias voltage at 50 MHz).

2.3. ATC/ACC feedback loops

As reported previously [22], similar electronic circuits were laid out with a Q spoiling resistor close to the cap and a microwave choke coil to introduce the biased DC voltage to the varactor diodes to change the tuning and coupling electronically. The typical beating rate of an isolated rat heart is about 5 Hz (300 bpm), therefore, the time constant of our AFC/ATC/ACC circuits should be set to a value of up to 20 ms that minimizes the motional noise without distortion to the EPR spectrum. In the AFC mode, a DC bias voltage from the AFC phase detector was taken as feed back to the oscillator to automatically stabilize the frequency of the microwave source. However, in the ATC mode, a DC bias voltage from the AFC phase detector was taken and connected to the tuning varactor diode. This signal from the AFC phase detector was used to adjust the resonance frequency of the resonator to the frequency of the oscillator. If the phasing was correct, the feedback circuit would lock the frequency of the resonator to the frequency of the oscillator automatically. Thus, the frequency of the resonator would be fixed even in the presence of sample motion.

A reference signal at a frequency of 20 kHz was provided from a SRS-850 lock-in amplifier (Stanford Research) to a mixer in order to modulate the incoming DC voltage corresponding to the detector-diode current of the bridge [22]. Then the modulated signal was fed back to the lock-in amplifier with filtering, phase adjustment, and amplification. After scaling in the voltage amplifier, this conditioned signal was connected to the coupling control varactor diode to adjust the coupling change due to the sample motion.

The time constant of the AFC module (Bruker) was fixed at 2 ms which was much less than the period of the cardiac cycle, 200 ms. The ATC circuit which was composed of a broadband amplifier didn't add any further restrictions to the AFC module. The only limiting step was the ACC circuit which was composed of the Lock-in

amplifier. However, the time constant of the Lock-in amplifier was set to a range of 1–100 ms depending on the motional frequency of the sample. With simulated phantom and beating rat heart experiments, the ATC/ACC system was shown to effectively respond to frequencies of up to 10 Hz with good suppression of noise from the moving phantom as well as moving biological objects.

The change of the frequency and coupling of the resonator with a beating rat heart in the sample arm were measured as less than 1 MHz and 1 dB, respectively. Therefore, the range of automatic tuning and automatic coupling were designed as ±5 MHz and 3 dB, respectively, to adequately accommodate the beating rat heart.

2.4. B_1 distribution and Q value of the resonator

With EPRI, one can map the B_1 distribution of the resonator. However, the perturbing sphere method is still needed to determine the B_1 value at the center of the resonator. Therefore, we chose to use the perturbing sphere method to map the B_1 field distribution [33]. In choosing the diameter of the sphere, as we have discussed previously [22], as long as the volume of the sphere is small compared to the volume of the sample arm of the resonator (it is 2.2% in our current design), the measurement should be accurate and the effect of the sphere on the B_1 field should be small. After the implementation of the ATC/ACC varactor diodes, the B_1 field distribution of the resonator was mapped with a brass sphere of diameter 5 mm inserted into the sample arm. When the resonator was inserted with a sample solution, the sphere was inserted into the solution and measurements were made inside the sample. As shown in Fig. 2, before loading, the resonator efficiency λ, defined as the ratio of B_1 over the square root of the incident power, W, was 0.018 mT/$(W)^{1/2}$ at the center of the resonator. The length with homogeneous B_1 field along the long axis was 50 mm (Fig. 2A, with closed circle and solid line), and the diameter of the cross section with homogeneous B_1 field was 20 mm (Fig. 2B, with closed circle and solid line). After inserted with 5 ml of 0.45% phosphate buffered saline (PBS) (a cylindrical volume with a diameter of 18 mm and a height of 20 mm), the resonator efficiency λ decreased to 0.013 mT/$(W)^{1/2}$ at the center of the resonator. The length with homogeneous B_1 field along the long axis decreased to 20 mm (Fig. 2A, with closed triangle and dashed line), and the diameter of the cross section with homogeneous B_1 field decreased to 18 mm (Fig. 2B, with closed triangle and dashed line). Within the sample, though the distribution of B_1 was less homogeneous than that of the resonator without sample, the homogeneity was still much better than that outside the sample volume. The mapping of the B_1 field demonstrated that the B_1 field was focused and concentrated inside the lossy sample.

The Q value of the resonator was measured while loading the resonator with different volumes of 0.45% PBS in an 18-mm id quartz tube using an Agilent 8719ES Network Analyzer. As shown in Fig. 3, when the resonator was empty, the Q value was 1100 (frequency 1.166 GHz). When the resonator was inserted with lossy samples, the Q value decreased to 400 even with a volume of only 0.5 ml. With increasing of the loading sample volume, the Q value decreased gradually. At a loading volume of 5 ml, the Q value was 150 at the frequency of 1.115 GHz.

2.5. Advantages over prior resonator designs

The current L-band TERR resonator with ATC and ACC provisions provides a number of advances over prior designs. While we have previously described an electronically tunable microwave resonator using a voltage-controlled piezoelectric actuator for adjustment of the resonance frequency via variations of the equivalent capacitance of the resonator, this design had no provision for ACC [21]. In our current design, we use varactor diodes to compensate for the changes in the tuning and coupling of the resonator due to the motional noise. The implemen-

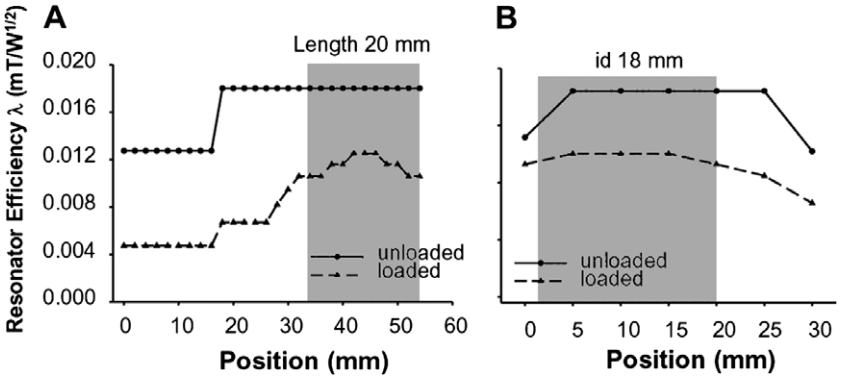

Fig. 2. B_1 field mapping of the L-band TERR resonator with a spherical brass ball of diameter 5 mm. (A) B_1 field distribution along the long axis of the resonator; the shaded area indicates the position and the length of the sample solution in the resonator. Of note, the points to the right of the sample area are not shown but are symmetrical with those to the left. (B) B_1 field distribution on the cross section of the resonator; the shaded area indicates the diameter of the sample solution. The closed circle and solid line: empty resonator, $f_0 = 1.167$ GHz, $Q = 1100$. The closed triangle and dashed line: resonator filled with 5 ml of 0.45% of PBS in a quartz tube of id 18 mm, od 20 mm, $f_0 = 1.115$ GHz, $Q = 150$.

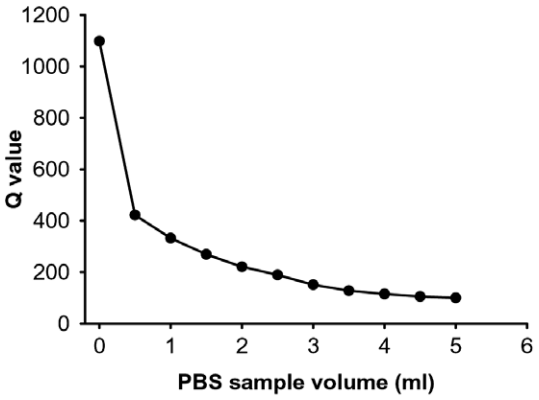

Fig. 3. Measurement of the Q value of the L-band TERR resonator. A quartz tube, 18 mm id, filled with different volume of PBS solution, was inserted into the sample arm of the resonator.

tation of varactor diodes improved the response of the tuning and coupling circuits since varactor diodes have much faster voltage response than that of piezoelectric actuators. Furthermore, the new resonator was constructed with capabilities of both electronic tuning and coupling.

This new resonator design also has several major advances compared to our previous design at 750 MHz [22]. The custom-designed smaller dimensions of the resonator sample arm and higher resonance frequency provided higher EPR sensitivity suitable for isolated rat heart imaging. The smaller sample dimensions and higher sensitivity required smaller dimensions of the varactor diodes used but with equally efficient dynamic range of voltage response for efficient quenching of motional noise-induced tuning and coupling variations. In the current design, we used a different varactor diode (MA4ST553-31, M/A-COM Inc.) but a similar normal total capacitance vs. reverse bias voltage response. This new varactor diode has only half of the size of the one previously used (MA4ST553-30, M/A-COM Inc.). The smaller varactor diodes allow better enclosure in the capacitive plate with less noise pickup from the modulation coils. Furthermore, the setup of the field modulation coils outside the sample arm rather than inside improved the sensitivity of the resonator. This required the design of slits on the wall to let modulation field penetrate through the copper clad resonator walls as depicted in Fig. 1B. Finally, the further distance of the modulation coils from the varactor diodes imposed less disturbance on the embedded varactor diodes in the wells under the tuning and coupling plates, and therefore reduces the baseline shift of the EPR spectrum.

3. Experimental methods

3.1. Chemicals

Solutions of 0.2 mM triarylmethyl, (TAM, OX063, a gift from Nycomed Innovation) in 0.45% PBS was prepared for phantom experiments. Oxygen sensitive spin probe lithium octa-*N*-butoxy-naphthalocyanine (LiNc-BuO) was synthesized as reported [34]. The redox probe nitroxyl radical 3-carbamoyl-proxyl (3-CP, Aldrich) was used with concentrations of 1 mM and 50 mM in Krebs perfusate.

3.2. Preparation of the isolated rat heart

Male Sprague–Dawley rats of weight 300 ± 30 g were used. After the rats were anesthetized with 50 mg/kg pentobarbital (ip), the thorax was opened and heparin (100 U) was given intravenously in the portal vein to prevent clotting. Then the heart was excised and the ascending aorta was cannulated. Retrograde perfusion was initiated by the method of Langendorff at a constant pressure of 80 mmHg using modified Krebs–bicarbonate-buffered perfusate containing (in mM): NaCl 120, KCl 5.9, $NaHCO_3$ 25, $MgCl_2$ 1.2, $CaCl_2$ 2.5, glucose 17, and EDTA 1. All perfusate solutions were filtered through two 1.2 μM Millipore filters and bubbled with 95% O_2 and 5% CO_2 gas mixture at 37 °C. A side arm in the perfusion line located proximal to the aortic cannula allowed the infusion of 3-CP solution. Contractile function was measured using a latex balloon inserted in the left ventricle (LV) and inflated with distilled water sufficient to produce an end diastolic pressure of 8–12 mmHg. For EPR/EPRI, the heart was perfused and transferred to a quartz tube of id of 16 mm. A polyethylene tube was inserted to the bottom of the quartz tube to perfuse the outside of the heart with warm buffer in order to keep the temperature at 37 °C. The flow of this buffer surrounding the heart was maintained 10-fold above that of the coronary flow. A suction tube was introduced in the quartz tube through the top rubber stop cock and the end opening of the tube was kept above the root of the aorta and the tube was connected to the vacuum system to maintain the liquid level in the quartz tube. In addition to keeping the temperature constant, the perfusate outside the heart served as a dampening media to the beating movement of the heart. For EPR imaging experiments, after 15 min of initial perfusion to allow the heart to reach stabilized contractile function as above, the heart was switched to a constant flow infusion of perfusate with 1 mM 3-CP at a rate of 2 ml/min that provided stable EPR intensity and EPR image data was collected.

3.3. Preparation of the phantom

The phantom was a glass bottle filled with 3 ml of 0.2 mM TAM in saline with NaCl concentration 0.45% (76.5 mM). The tube was mounted to the end of a quartz rod, which provided the actuator movement from an 8 ohm audio speaker [22,30]. Signals of variable frequency and amplitude from a function generator (Arbitrary Waveform Generator Model No. 75, Wavetek) were used to control the frequency (f, Hz) and excursion (A, mm) of the

phantom motion to simulate the motion of a moving object such as a beating rat heart.

3.4. EPR/EPRI spectrometer setup

A custom-made L-band EPR imaging system was used to perform the spectroscopy and imaging experiments. This system contained a fixed frequency microwave bridge as described previously [21,35]. The imaging system was equipped with a set of three-dimensional field gradient coils with gradient capability of up to 1200 mT/m along each axis. The software for data acquisition and image reconstruction was as described [36]. Nitroxyl radicals give a three-line EPR spectrum. For EPRI, the low-field peak was used with forward-subtraction hyperfine correction [37]. The EPR/EPRI parameters were as follows: for TAM and LiNc-BuO spectroscopy: microwave power 5 mW ($B_1 = 9.2 \times 10^{-4}$ mT), modulation amplitude 1×10^{-2} mT, scan width 1 mT, scan time 15 s, time constant 80 ms; for EPRI: microwave power 32 mW ($B_1 = 5.9 \times 10^{-3}$ mT), gradient field 50 mT/m, modulation amplitude 7×10^{-2} mT, scan width 1.5 mT, spatial window $30 \times 30 \times 30$ mm^3.

4. Experimental results

4.1. EPR spectroscopy

The resonator changes due to sample motion induced distortion in the spectrum. We call this kind of distortion to the spectrum motional noise. Disturbance to the coupling of the resonator was manifested on the baseline and the spectrum. However, the disturbance to the tuning of the resonator was manifested only on the EPR signal, not on the baseline. In a beating heart, the motion induced not only baseline noise that reduced the signal to noise ratio, but also frequency instability that perturbed the accuracy of EPR line-width and line-shape measurement. The latter was particularly a problem for EPR oximetry that relied upon precise line-width measurements to determine tissue oxygen tension. The current design of the L-band TERR resonator with ATC/ACC provisions should automatically quench motion-induced noise and enable the accurate measurement of the EPR signal and its line-width in a beating phantom or heart. In order to test the capability of the resonator to quench the motional noise, a moving sample, of 3 ml of 0.2 mM TAM in 0.45% PBS, was tested [22,30]. Fig. 4 shows the EPR spectra of the phantom attached to the end of a quartz tube that was fixed to the pivot center of an 8 W speaker. By changing the audio signal amplitude and frequency, the excursion of the sample was adjusted to simulate different moving frequency and amplitude. With the ATC/ACC provisions, EPR spectra were obtained and the moving noise was dramatically decreased. As shown in the figure, when the control circuit was configured in the AFC mode and there was no movement from the phantom ($f = 0$ Hz, $A = 0$ mm), the

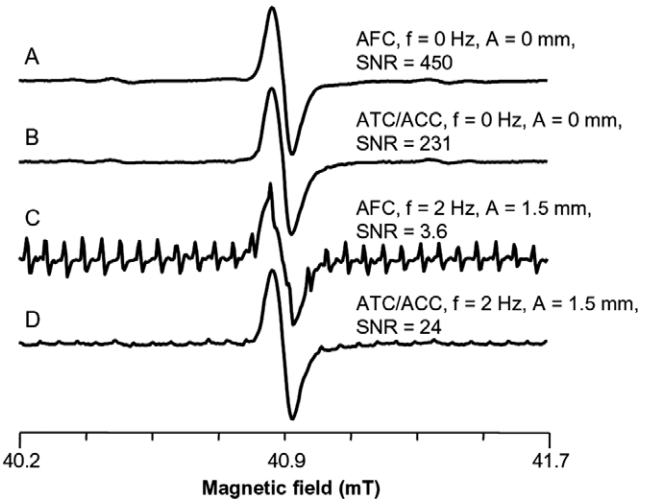

Fig. 4. Improvement of the S/N of EPR spectrum with the ATC/ACC provisions. The EPR spectra were taken from a phantom of 3 ml of 0.2 mM TAM in 0.45% PBS solution. The phantom was set to periodic motion in the resonator with a frequency of f (Hz) and an excursion of A (mm). Frequency control was switched between AFC and ATC/ACC with (A) AFC, $f = 0$ Hz, $A = 0$ mm; (B) ATC/ACC, $f = 0$ Hz, $A = 0$ mm; (C) AFC, $f = 2$ Hz, $A = 1.5$ mm; (D) ATC/ACC, $f = 2$ Hz, $A = 1.5$ mm. A 6.7-fold of improvement in S/N was achieved with ATC/ACC provisions.

S/N was measured as 450 (Fig. 4A). When the two ATC/ACC feed-back circuits were connected, the S/N was 231, approximately two times (1.9) lower which was consistent with our previous report (Fig. 4B) [22]. This reduction of S/N upon insertion of the varactor diodes and the supporting circuits was due to the controlling circuits as well as some possible leakage of the 100 kHz field modulation signal into the varactor diode circuits which was manifested as a slight increase of the baseline offset on the EPR spectrum. Once electronically biased, the Q value of the varactor diodes decreases and this may also contribute to the reduction of the S/N of the EPR spectrum. When there was a perturbation with a frequency of 2 Hz and amplitude of 1.5 mm, the S/N was only 3.6 in the AFC configuration (Fig. 4C). However, with the implement of ATC/ACC provisions, the S/N was improved to 24, a 6.7-fold increase (Fig. 4D). We also observed that the line-width and the line shape were completely restored after ATC/ACC with motional noise compared to that of AFC and ATC/ACC without motional noise.

After validation of the ATC/ACC setup with the moving phantom experiments, the resonator was applied for EPR spectroscopy on the isolated perfused rat heart. About 10 μg of LiNc-BuO microcrystal was implanted with a 25-G needle in the mid myocardium of the anterior wall of the LV. Then the heart was perfused and transferred to the quartz tube and immersed in the perfusate to the level of the aorta to keep the temperature constant. Then EPR spectroscopy was performed.

As shown in Fig. 5, with AFC configuration, the beating heart gave a very noisy spectrum with S/N of 2 (Fig. 5A). It was very difficult and inaccurate to measure the EPR line-

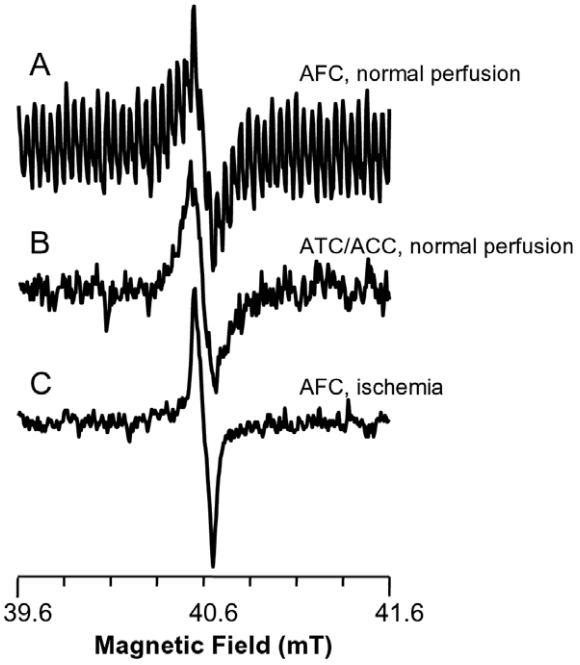

Fig. 5. Improvement of the EPR spectral S/N from an isolated beating rat heart. About 10 μg of LiNc-BuO microcrystal was implanted in the mid myocardium in the anterior wall of the left ventricle. The EPR spectra were taken with and without ATC/ACC: (A) AFC, beating heart; (B) ATC/ACC, beating heart; (C) AFC, ischemic heart. A 4-fold of improvement in S/N was achieved with ATC/ACC provisions.

width from this noisy spectrum. When the ATC/ACC provisions were implemented, a much cleaner spectrum was obtained with S/N of 8. When the heart was subjected to global ischemia therefore beating was stopped, the spectrum with AFC showed an S/N of 10. From these spectra, it was demonstrated that a 4-fold improvement of S/N was achieved on the isolated beating rat heart when the ATC/ACC feedback loops were implemented. This improvement of the S/N enabled the accurate measurement of the EPR line-width.

4.2. EPR imaging

With appropriate selection of redox probes, EPR imaging provides a powerful technique to map the redox distribution in the myocardium of a beating rat heart. However, the beating-induced noise degraded the quality of the projection data when the EPR spectrometer was configured in the AFC mode. With the ATC/ACC provisions in the current resonator, EPR imaging data can be obtained with improved S/N on a beating rat heart. Fig. 6A shows the zero-gradient projection obtained with AFC ($S/N \sim 1$). As shown in Fig. 6D, the noise was greatly decreased with implementation of ATC/ACC ($S/N \sim 6$). Fig. 6B shows the photograph of the isolated beating rat heart with the aortic cannula and the balloon inserted in the left ventricle. Fig. 6C shows that with AFC only a very noisy 3D EPR image was obtained with no recognizable heart structure. With ATC/ACC, however, as shown in Fig. 6E, much improved 3D EPR images of the beating heart were obtained as can be seen in the full surface rendered image and the vertical and horizontal cutouts. The overall shape of the heart and the void space of the balloon in the left ventricle, LV, can be seen. These 3D EPR images show a relatively homogeneous spatial distribution of the 3-CP probe in the myocardium. The two 2D cutout images clearly show the LV as a void space at the position of the

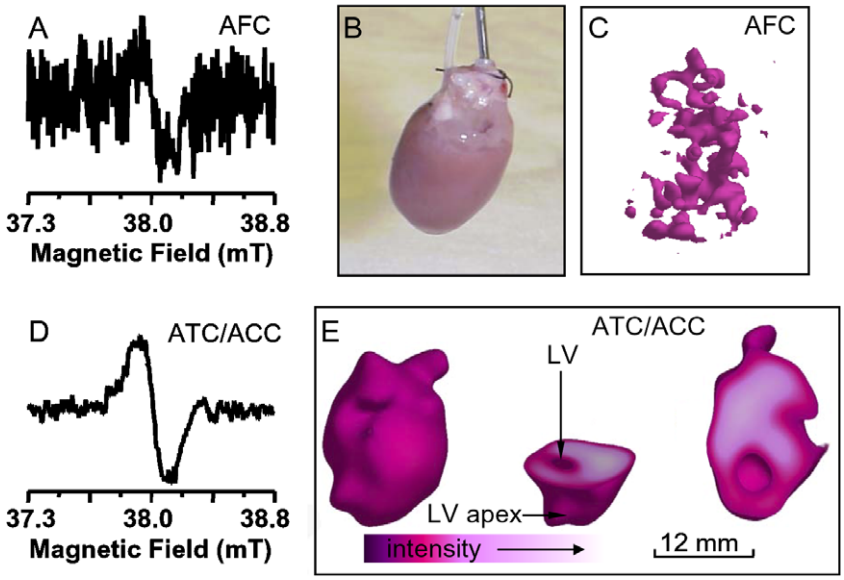

Fig. 6. 3D EPR imaging of the perfused beating rat heart. The heart was perfused with 1 mM 3-CP in perfusate with a rate of 2 ml/min. The low-field peak was used to perform the imaging. (A) Zero-gradient projection with AFC; (B) photograph of the heart; (C) 3D image of the heart with AFC; (D) zero-gradient projection with ATC/ACC; (E) 3D image and the two 2D cutouts of the heart. Legend: LV, left ventricle; AFC, automatic frequency control; ATC/ACC, automatic tuning and coupling control. These experiments demonstrated a dramatic improvement of the EPR images with ATC/ACC on the distribution of nitroxyl radical in the beating heart.

inserted balloon. Of note, in these experiments the heart is beating at a rate of ~5 Hz and without gating this causes some blurring of the heart surface and features visualized. These measurements demonstrated the capability of the ATC/ACC provisions and L-band TERR to provide the stable resonator tuning and coupling required for 3D spatial EPR imaging of free radicals in the heart.

5. Summary and conclusions

An L-band TERR resonator with ATC/ACC provisions was constructed and evaluated for EPR spectroscopy and imaging on a moving phantom and an isolated beating rat heart. In general, samples with diameter up to 22 mm and volume up to 15 ml can be studied with this resonator design. In the sample arm, the homogeneous length of B_1 field along the long axis was 50 mm and the diameter of the homogeneous cross section of B_1 field was 20 mm. The Q value of the resonator without sample was very high (1100). When the resonator was filled with a lossy sample such as half-water half-saline, the Q value dropped to 400 at a loading volume of 0.5 ml and then to 150 at a volume of up to 5.0 ml. With sample present, the B_1 field intensity was decreased and concentrated within the sample.

Upon the introduction of ATC/ACC circuits, a 1.9-fold increase in noise level was introduced and this was consistent with our prior report [22]. When EPR spectroscopy was applied to moving objects, the resonator improved the S/N 6.7 times on a moving phantom of TAM solution, 6 times on a beating heart globally infused with nitroxyl radical and 4 times on a beating heart with point implantation of the oxygen sensitive probe LiNc-BuO. The improvement seen in S/N was dependent upon the severity of motion induced noise with greater improvements seen with higher noise severity. This resonator design with ATC/ACC provisions was applied to perform 3D spatial EPR imaging of the perfused beating rat heart and was highly effective in reducing motion induced noise enabling 3D mapping of the localization of free radicals in the beating heart.

In conclusion, the L-band TERR with ATC and ACC, enables EPR spectroscopy and imaging measurements on the isolated beating rat heart. It allows accurate measurement of the EPR line-width of an oximetry probe and imaging of the spatial distribution of free radicals in beating rat hearts. Thus, this resonator design with ATC/ACC capability enables greatly improved EPR measurements of tissue oxygenation and free radical distribution and metabolism in the isolated beating rat heart. It should be a useful tool enabling studies that will add new knowledge to our current understanding of cardiac physiology and disease.

Acknowledgments

We thank Dr. Periannan Kuppusamy for providing the oxygen sensitive probe LiNc-BuO and for helpful advice. This work was supported by NIH Grants EB00306, EB00890 (J.L.Z.), and 0435299N, HL081630 (G.H.).

References

[1] L.J. Berliner, H. Fujii, Magnetic resonance imaging of biological specimens, Science 227 (1985) 517–519.
[2] H.J. Halpern, M. Peric, C. Yu, E.D. Barth, G.V. Chandramouli, M.W. Makinen, G.M. Rosen, In vivo spin-label murine pharmacodynamics using low-frequency electron paramagnetic resonance imaging, Biophys. J. 71 (1996) 403–409.
[3] M.C. Krishna, N. Devasahayam, J.A. Cook, S. Subramanian, P. Kuppusamy, J.B. Mitchell, Electron paramagnetic resonance for small animal imaging applications, Ilar J. 42 (2001) 209–218.
[4] G.R. Eaton, A new EPR methodology for the study of biological systems, Biophys. J. 64 (1993) 1373–1374.
[5] H.M. Swartz, S. Boyer, P. Gast, J.F. Glockner, H. Hu, K.J. Liu, M. Moussavi, S.W. Norby, N. Vahidi, T. Walczak, et al., Measurements of pertinent concentrations of oxygen in vivo, Magn. Reson. Med. 20 (1991) 333–339.
[6] G. He, R.A. Shankar, M. Chzhan, A. Samouilov, P. Kuppusamy, J.L. Zweier, Noninvasive measurement of anatomic structure and intraluminal oxygenation in the gastrointestinal tract of living mice with spatial and spectral EPR imaging, Proc. Natl. Acad. Sci. USA 96 (1999) 4586–4591.
[7] J.A. Brivati, A.D. Stevens, M.C.R. Symons, A radiofrequency ESR spectrometer for in vivo imaging, J. Magn. Reson. 92 (1991) 480–489.
[8] M. Alecci, S.J. McCallum, D.J. Lurie, Design and optimization of an automatic frequency control system for a radiofrequency electron paramagnetic resonance spectrometer, J. Magn. Reson. 117 (1995) 272–277.
[9] S.J. McCallum, M. Alecci, D.J. Lurie, Modification of a whole-body NMR imager into a radiofrequency EPR spectrometer suitable for in vivo measurements, Meas. Sci. Technol. 7 (1996) 1012–1018.
[10] H. Hirata, Y. Yamaguchi, T. Takahashi, Z.W. Luo, Control characteristics of an automatic matching control system for in vivo EPR spectroscopy, Magn. Reson. Med. 50 (2003) 223–227.
[11] L.J. Berliner, in: L.J. Berliner (Ed.), Biological Magnetic Resonance, vol. 18, Kluwer Academic/Plenum Publishers, Dordrecht, Netherlands, 2003.
[12] C.J. Bender, EPR: instrumental methods, in: C.J. Bender, L.J. Berliner (Eds.), Biological Magnetic Resonance, Kluwer Academic/Plenum Publishers, Dordrecht, Netherlands, 2004.
[13] P. Kuppusamy, M. Chzhan, K. Vij, M. Shteynbuk, D.J. Lefer, E. Giannella, J.L. Zweier, Three-dimensional spectral-spatial EPR imaging of free radicals in the heart: a technique for imaging tissue metabolism and oxygenation, Proc. Natl. Acad. Sci. USA 91 (1994) 3388–3392.
[14] J.L. Zweier, P. Kuppusamy, Electron paramagnetic resonance measurements of free radicals in the intact beating heart: a technique for detection and characterization of free radicals in whole biological tissues, Proc. Natl. Acad. Sci. USA 85 (1988) 5703–5707.
[15] J.L. Zweier, P. Kuppusamy, R. Williams, B.K. Rayburn, D. Smith, M.L. Weisfeldt, J.T. Flaherty, Measurement and characterization of postischemic free radical generation in the isolated perfused heart, J. Biol. Chem. 264 (1989) 18890–18895.
[16] W. Froncisz, J.S. Hyde, The loop-gap resonator: a new microwave lumped circuit ESR sample structure, J. Magn. Reson. 47 (1982) 515–521.
[17] J.S. Hyde, W. Froncisz, Loop-gap resonators, Electron Spin Resonance 10A (1986) 175–184.
[18] R. Diodato, M. Alecci, J.A. Brivati, V. Varoli, A. Sotgiu, Optimization of axial RF field distribution in low-frequency EPR loop-gap resonators, Phys. Med. Biol. 44 (1999) N69–N75.
[19] G.A. Rinard, R.W. Quine, G.R. Eaton, An L-band crossed-loop (Bimodal) EPR resonator, J. Magn. Reson. 144 (2000) 85–88.

[20] H. Hirata, T. Walczak, H.M. Swartz, Electronically tunable surface-coil-type resonator for L-band EPR spectroscopy, J. Magn. Reson. 142 (2000) 159–167.
[21] M. Chzhan, P. Kuppusamy, J.L. Zweier, Development of an electronically tunable L-band resonator for EPR spectroscopy and imaging of biological samples, J. Magn. Reson. B 108 (1995) 67–72.
[22] G. He, S. Petryakov, A. Samouilov, M. Chzhan, P. Kuppusamy, J.L. Zweier, Development of a resonator with automatic tuning and coupling capability to minimize sample motion noise for in vivo EPR spectroscopy, J. Magn. Reson. 149 (2001) 218–227.
[23] H. Hirata, Z.W. Luo, Stability analysis and design of automatic frequency control system for in vivo EPR spectroscopy, Magn. Reson. Med. 46 (2001) 1209–1215.
[24] V. Krymov, G.J. Gerfen, Analysis of the tuning and operation of reflection resonator EPR spectrometers, J. Magn. Reson. 162 (2003) 466–478.
[25] H. Hirata, H. Watanabe, M. Kumada, K. Itoh, H. Fujii, Decoupling of automatic control systems in a continuous-wave electron paramagnetic resonance spectrometer for biomedical applications, NMR Biomed. 17 (2004) 295–302.
[26] R.P. de Alejo, C. Garrido, P. Villa, I. Rodriguez, J.J. Vaquero, J. Ruiz-Cabello, M. Cortijo, Automatic tuning and matching of a small multifrequency saddle coil at 4.7T, Magn. Reson. Med. 51 (2004) 869–873.
[27] R.D. Venook, B.A. Hargreaves, G.E. Gold, S.M. Conolly, G.C. Scott, Automatic tuning of flexible interventional RF receiver coils, Magn. Reson. Med. 54 (2005) 983–993.
[28] L.T. Muftuler, G. Gulsen, K.D. Sezen, O. Nalcioglu, Automatic tuned MRI RF coil for multinuclear imaging of small animals at 3T, J. Magn. Reson. 155 (2002) 39–44.
[29] P. Kuppusamy, P. Wang, A. Samouilov, J.L. Zweier, Spatial mapping of nitric oxide generation in the ischemic heart using electron paramagnetic resonance imaging, Magn. Reson. Med. 36 (1996) 212–218.
[30] P. Kuppusamy, M. Chzhan, P. Wang, J.L. Zweier, Three-dimensional gated EPR imaging of the beating heart: time-resolved measurements of free radical distribution during the cardiac contractile cycle, Magn. Reson. Med. 35 (1996) 323–328.
[31] P. Kuppusamy, P. Wang, J.L. Zweier, Three-dimensional spatial EPR imaging of the rat heart, Magn. Reson. Med. 34 (1995) 99–105.
[32] H.J. Halpern, D.P. Spencer, J. Polen, K.K. Bowman, A.C. Nelson, E.M. Dowey, B.A. Teicher, Imaging radio frequency electron-spin-resonance spectrometer with high resolution and sensitivity for in vivo measurements, Rev. Sci. Instrum. 60 (1989) 1040–1050.
[33] J.H. Freed, D.S. Leniart, J.S. Hyde, Theory of saturation and double resonance effects in ESR spectra. III. RF coherence and line shapes, J. Chem. Phys. 47 (1967) 2762–2773.
[34] R.P. Pandian, N.L. Parinandi, G. Ilangovan, J.L. Zweier, P. Kuppusamy, Novel particulate spin probe for targeted determination of oxygen in cells and tissues, Free Radic. Biol. Med. 35 (2003) 1138–1148.
[35] M. Chzhan, P. Kuppusamy, A. Samouilov, G. He, J.L. Zweier, A tunable reentrant resonator with transverse orientation of electric field for in vivo EPR spectroscopy, J. Magn. Reson. 137 (1999) 373–378.
[36] P. Kuppusamy, M. Chzhan, J.L. Zweier, Development and optimization of three-dimensional spatial EPR imaging for biological organs and tissues, J. Magn. Reson. B 106 (1995) 122–130.
[37] P. Kuppusamy, J.L. Zweier, A forward-subtraction procedure for removing hyperfine artifacts in electron paramagnetic resonance imaging, Magn. Reson. Med. 35 (1996) 316–322.